Thermal treatment of Cs-exchanged chabazite by hot isostatic pressing to support decommissioning of Fukushima Daiichi Nuclear Power Plant

Laura J. Gardner[1], Sam A. Walling[1], Claire L. Corkhill[1] and Neil C. Hyatt[1*]

[1]*NucleUS Immobilisation Science Laboratory, Department of Materials Science and Engineering, University of Sheffield, Sir Robert Hadfield Building, Sheffield, S1 3JD, UK*

**To whom correspondence should be addressed. Email: n.c.hyatt@sheffield.ac.uk*

ABSTRACT

Ion exchange materials are used widely for the removal of radionuclides from contaminated water at nuclear licensed sites, during normal operating procedures, decommissioning and in accident clean-up, such as the ongoing recovery operation at the Fukushima Daiichi nuclear power plant. Framework silicate inorganic ion exchange materials, such as chabazite ($(Na_{0.14}K_{1.03}Ca_{1.00}Mg_{0.17})[Al_{3.36}Si_{8.53}O_{24}]\cdot 9.7H_2O$), have shown particular selectivity towards ^{137}Cs uptake, but their safe storage poses a number challenges requiring conditioning into passively safe waste packages of minimal volume. We demonstrate the transformation of Cs-exchanged chabazite into a glass-ceramic wasteform by hot isostatic pressing to produce a durable consolidated monolith. The application of heat and pressure resulted in the collapse of the chabazite framework, forming crystalline Cs-substituted leucite ($Cs_{0.15(3)}K_{0.57(4)}Al_{0.90(4)}Si_{2.24(5)}O_6$) incorporated within a K_2O-CaO-MgO-Al_2O_3-SiO_2 glass. The Cs partitioned preferentially into the Cs/K-feldspar which incorporated ~77% of the Cs_2O inventory. Analysis of the chemical durability of the glass-ceramic wasteform revealed that the Cs release rates were comparable or lower than those reported for vitrified high level and intermediate level wastes. Overall, hot isostatic pressing was demonstrated to be an effective processing technology for conditioning spent inorganic ion exchange materials by yielding durable and passively safe wasteforms.

Key Words: Hot isostatic pressing, ion exchange materials, nuclear waste management, characterisation, chemical durability

1. Introduction

On March 11th, 2011, the Great East Japan earthquake (9.0 magnitude) occurred, which resulted in the automatic shutdown of the operating reactors (Units 1-3) at the Fukushima Daiichi nuclear power plant (NNP) [1, 2]. In the series of events that followed, the nuclear fuel melted with the cladding and there were a series of hydrogen explosions in Units 1, 3 and 4 [1]. To cool the damaged reactor cores and remove residual decay heat, sea water was injected into the reactor buildings and turbine halls using fire trucks for approximately two weeks, after which fresh water circulation was reinstated with restored access to the power supply [3]. The emergency and post-accident reactor cooling resulted in the generation of large volumes of highly radioactive water (due to contact with molten/damaged fuel) of which ^{137}Cs is the largest component of the total activity [3]. ^{137}Cs is a short-lived radionuclide ($t_{1/2}$ = 30.2 years) that poses a radiological risk to humans and the environment, due to high energy beta and gamma emissions (^{137}Cs beta decay to ^{137m}Ba (0.512 MeV) followed by gamma decay to ^{137}Ba (0.662 MeV)) [4], the ease of exchange for K and Na salts in biological organisms, and its high solubility in water.

To facilitate ^{137}Cs removal from the contaminated coolant water, two water treatment facilities were installed on the Fukushima Daiichi NPP site, Kurion and SARRY, which used the framework silicate inorganic ion exchange materials herschelite [5] and IONSIV (Honeywell UOP [6]). These facilities have since treated contaminated water volumes of 394,720 m^3 and 1,827,290 m^3, respectively [7] (values correct as of April 2020). Similar framework silicate ion exchange materials are used in the routine treatment of radionuclide contaminated water at nuclear licensed sites, for example, the SIXEP plant at Sellafield (UK).

After selective uptake of radionuclides, the storage of spent ion exchange materials poses several challenges. This is particularly the case at Fukushima Daiichi NPP where on-site storage space is extremely limited, and there are strong incentives for the rapid decommissioning of the site. Spent ion exchange materials pose a particular challenge, due to: potential dispersal in the event of a loss of containment, as a result of their granular nature; very high dose rates and radiogenic heating, as a result of their selectivity for short-lived radionuclides (e.g. ^{90}Sr, ^{137}Cs); and production of hydrogen from the radiolysis of entrained water, which poses a potential explosion risk [8]. Since spent ion exchange materials are generated not only at Fukushima, but also at other nuclear licenced sites as described above, there is a clear need to develop suitable conditioning routes to minimise the risk associated with these highly radioactive and

dispersible materials, whilst producing passively safe waste packages of minimal volume, to reduce storage and disposal costs.

One potential conditioning route for spent ion exchange materials is to apply hot isostatic pressing (HIPing), which uses the concurrent application of temperature (up to 2200 °C) and pressure (typically 100-200 MPa) to a work-piece (HIP canister) within a pressure vessel. The changes imposed to the work-piece include the conversion into a passively safe solid monolith product, with exclusion of porosity and voidage (with respect to powder and granular materials) [9]. For these reasons, HIPing is currently under consideration as a thermal treatment process for conditioning radioactive wastes ranging from sludges [10, 11] and high level wastes [12, 13] to portions of the UK Pu stockpile [14-17]. Typically, the resulting HIPed wasteform will be a ceramic or glass-ceramic matrix, where the waste is an integral component of the host matrix [18, 19]. HIPing radioactive waste provides several advantages: the batch to batch processing provides inventory and criticality control, where desirable; it is possible to achieve high waste loadings by conversion of adequately dried waste directly to a monolith of acceptable phase assemblage; there is no requirement for a fluid melt, as in the application of conventional vitrification; and there is minimal off-gas and secondary waste generated, due to the hermetically sealed nature of the HIP can. There is potential for waste volume reduction between 20-70%, which could provide significant storage and disposal cost savings [18, 19]. In principle, a single HIP unit could also process multiple waste feeds, due to the batch wise and contained nature of the process and the wide range of accessible process conditions [19].

At present, there are no full-scale HIP plants operational for nuclear waste treatment, however the Australian Nuclear Science and Technology Organisation (ANSTO) are commissioning a HIP plant (Synroc Waste Treatment Plant; SWTF) that is expected to be completed in 2020, with an estimated annual capacity to process ~5000 L of wastes generated from medical isotope production [20]. The UK Nuclear Decommissioning Authority (NDA) have proposed HIPing as a credible option for processing a portion of the civil PuO_2 stockpile [21] (and plutonium-residues) with several research programmes underway. In the USA, the Department of Energy (DoE) have considered HIPing for conditioning calcined high level wastes generated at the Idaho Nuclear Technology and Engineering Center (INTEC) from spent fuel reprocessing operations. HIPing INTEC calcined wastes is reported to be capable of saving an estimated $2 billion in disposal costs, which is equivalent to a 50% reduction when compared with the baseline immobilisation

89 option of a borosilicate glass matrix (based on analysis reported in 2004) [12]. As such, there is a clear
90 mandate and need to continue underpinning HIP wasteform characterisation and performance for a wide
91 variety of nuclear wastes (including spent ion exchange materials investigated here) to enable/assist
92 waste management decisions by appropriate governmental bodies and waste owners.

93 In this study, the application of HIPing as a consolidation technique for the conversion of Cs-exchanged
94 inorganic ion exchange material was demonstrated based on small-scale (~35 g) wasteforms, which
95 resulted in a multiphase glass-ceramic at 70 wt. % waste loading. Cs-exchanged chabazite
96 ($(Na_{0.14}K_{1.03}Ca_{1.00}Mg_{0.17})[Al_{3.36}Si_{8.53}O_{24}]\cdot 9.7H_2O$), which is reasonably similar in composition to herschelite
97 ($(Na_2,K_2,Ca,Sr,Mg_2)[Al_2Si_4O_{12}]_2\cdot 12H_2O$) deployed by Kurion (now part of Veolia Nuclear Solutions) at
98 Fukushima Daiichi NPP [3]) was employed to simulate this waste. The HIP parameters were optimised by
99 the variation of pressure (50-100 MPa) and temperature (1050-1250 °C) at a fixed duration (4 h) and the
100 resulting small-scale wasteform was characterised by XRD, XRF and SEM/EDX techniques and, to assess
101 its passive safety, a durability assessment was performed.

102

2. Experimental Methodology

2.1 Materials and Methods

Natural chabazite was sourced as the product "Zeover" from Verdi S.p.A. The particle size range was 0.1 to 0.7 mm, the overall composition was $(Na_{0.14}K_{1.03}Ca_{1.00}Mg_{0.17})[Al_{3.36}Si_{8.53}O_{24}]\cdot 9.7H_2O$ with a cation exchange capacity (CEC) of 2.2 ± 0.2 meq/g [22]. However, being derived from a natural source, 70% of the material was chabazite, with the remaining fraction including contributions from: volcanic glass (18%); phillipsite (2%); K-feldspar (5%); biotite (2%) and; pyroxene (3%) [22]. The natural chabazite in this proof of concept study was previoulsy utilised in vitrification studies as a reasonable simulant of a proprietary ion exchange deployed by Kurion (now part of Veolia Nuclear Solutions) [23]. Therefore, the HIPed wasteforms developed here could be relevant to the processing of spent high dose materials at Fukushima Daiichi NPP, at a 70 wt. % waste loading (chabazite) with approximately 30 wt. % additives of suitable composition (as a mixture of oxides or precursor glass frit), as decribed above.

Chabazite (250 g) was ion-exchanged using a solution of 0.1 M $^{133}CsNO_3$ (Sigma Aldrich, 99% purity) dissolved in ultrapure deionized H_2O (18.2 MΩ) to simulate ion exchange operations at nuclear licensed sites. The ion-exchange solution and chabazite were equilibrated on a roller mill for 24 h at room temperature, after which the exchange solution was replaced and the process repeated for a second exchange (cumulative 48 h exchange). The ion exchanged chabazite, hereafter referred to Cs-chabazite, was vacuum filtered and washed three times using 1 L of distilled H_2O. The Cs-chabazite was dried at 95 °C for 48 h, the resulting material had a Cs_2O concentration of 2.88 ± 0.07 wt. % (determined *via* fused bead X-ray Fluorescence (XRF) spectroscopy, Table 1), which was equivalent to 0.72 ± 0.02 mol. %. The Cs uptake within chabazite was calculated to be 0.27 meq/g after a 48 h exchange period, which was equivalent to a Cs loading of ~12%, based on the CEC for this natural source material. This is considered reasonably representative of the operational deployment of this material, which does not target complete exchange of Cs to the maximum sorption capacity, so as to maintain a high decontamination factor and to enable the spent ion exchange material to be managed within acceptable dose rate constraints. The exchange process occurred predominately with Ca (with minor changes for K, Mg and Na); CaO, decreased from 8.23 ± 0.07 mol. % (as-received) to 7.68 ± 0.06 mol. % in the Cs-exchanged chabazite (Table 1). The reported selectivity of chabazite (based on the Gibbs free energies of exchange) follows the order: Cs^+ >

131 $K^+ > Rb^+ > Na^+ = Ba^{2+} > Sr^{2+} > Ca^{2+} > Li^+$ [24, 25], which is broadly in agreement with our reported XRF data
132 (Table 1).

133 **Table 1.** XRF oxide composition of as-received chabazite and Cs-chabazite (errors indicated in parenthesis)

Oxide	Wt. %		Mol. %	
	As-received	Cs-chabazite	As-received	Cs-chabazite
Al_2O_3	20.25 (± 0.06)	19.57 (± 0.10)	13.72 (± 0.03)	13.56 (± 0.06)
CaO	6.68 (± 0.03)	6.09 (± 0.05)	8.23 (± 0.02)	7.68 (± 0.06)
Cs_2O	0.00 (± 0.00)	2.88 (± 0.07)	0.00 (± 0.00)	0.72 (± 0.02)
Fe_2O_3	5.48 (± 0.01)	5.46 (± 0.03)	2.37 (± 0.01)	2.42 (± 0.01)
K_2O	7.20 (± 0.03)	7.00 (± 0.07)	5.28 (± 0.04)	5.25 (± 0.06)
MgO	2.08 (± 0.02)	2.08 (± 0.01)	3.57 (± 0.04)	3.64 (± 0.03)
Na_2O	0.89 (± 0.01)	0.85 (± 0.01)	1.00 (± 0.01)	0.96 (± 0.01)
SiO_2	56.73 (± 0.31)	55.38 (± 0.05)	65.24 (± 0.07)	65.15 (± 0.01)
TiO_2	0.69 (± 0.02)	0.70 (± 0.02)	0.59 (± 0.01)	0.62 (± 0.02)

134

135 Thermal analysis and mass spectroscopy data were collected on the as-received chabazite using a Perkin
136 Elmer TGA 4000 instrument in conjunction with a HPR-20 QIC benchtop Gas Analysis System (MS) using
137 alumina crucibles under a N_2 atmosphere; the sample was heated to 1000 °C at a ramp rate of 10 °C/min.
138 All HIP samples were pre-calcined to remove water at 300 °C for 12 h in a muffle furnace prior to HIP
139 canister packing. Immediately following the pre-calcination step, ~35 g of Cs-chabazite was packed into
140 each HIP canister (manufactured in-house using 316 stainless steel) using a hydraulic press to increase the
141 packing density and, thus, the waste loading per HIP canister. Following this, each canister was qualified
142 for HIPing through a two-step evacuation and bake-out verification process. This involved evacuating the
143 HIP canister until a vacuum of <8 Pa was achieved, followed by exposure to 300 °C until the initial vacuum
144 recovered, at which point, the canister was crimped and sealed (welded) to create a hermetically sealed
145 work piece. These stages remove excess volatiles/water from the canister, which could have a deleterious
146 effect on the densification achieved and lead to porosity in the HIPed wasteform [14, 26].

147 To determine the effectiveness of hot isostatic pressing (HIPing) as a thermal treatment application for
148 ion exchange materials, Cs-chabazite was HIPed at 1050 °C, 1150 °C and 1250 °C under two pressure

regimes, 100 MPa and 50 MPa ($Ar_{(g)}$ used as the pressurising media) with a fixed 4 h dwell period using the AIP-630H research HIP at the University of Sheffield. Our choice of processing temperature was governed by prior studies on high temperature treatment of ion exchange materials, which demonstrated collapse and reaction of the aluminosilicate framework in the range 1000-1300 °C [27-29]. The HIPed canisters were sectioned using a Buehler Abrasimet 250 saw and the extracted monoliths were further sectioned for analysis using a Buehler Isomet 100 saw. Powder X-ray diffraction patterns were collected between 5° < 2θ < 50° using a Bruker D2 Phaser diffractometer with a Lynxeye detector and Ni filtered Cu K_α radiation (1.5418 Å) using a step size of 0.02° 2θ and a count time of 1 s per step. Scanning Electron Microscopy (SEM) images were collected using a low vacuum Hitachi TM3030 analytical benchtop SEM with an integrated Bruker EDX system (Quantax 70) at 15 kV and a ~7.0 mm working distance on polished (1 µm diamond finish) and carbon coated specimens. Reported semi-quantitative compositions were calculated based on the average of 10 spot analyses per phase with assumed oxygen stoichiometry (due to the low accuracy of EDX for oxygen determination).

A durability assessment was performed using with ASTM C1285 methodology (PCT-B) [30]. Samples were crushed and sieved to a size fraction of 150 – 75 µm and washed several times with isopropanol alcohol to remove residual fines from the fraction. The desired sample mass was added to pre-cleaned PFA vessels with 10 mL of ultrapure deionized H_2O (18.2 MΩ) to achieve a surface area to volume ratio of 2000 m^{-1}. The vessels were prepared in triplicate with duplicate blanks (ultrapure deionised H_2O only) and placed within an oven at 90 ± 1 °C, with vessels being sacrificed for sampling at 1, 3, 7, 14 and 28 days. For each time point, vessels were allowed to cool to room temperature before recording the total vessel mass (to calculate evaporative loss) and monitoring the pH. An aliquot of the leachate was removed from each vessel, filtered using a 0.2 µm cellulose acetate syringe filter and acidified using high purity nitric acid (Fisher Scientific, Ultrapure NORMATOM, 67-69% HNO_3). The elemental concentration of Cs was determined using by Inductively Coupled Plasma-Mass Spectroscopy (ICP-MS, Thermo Fisher Scientific iCAP RQ), all other elements were measured using an Inductively Coupled Plasma-Optical Emission Spectrometer (ICP-OES, Thermo Fisher Scientific iCAP Duo6300). The reported data were normalised to the surface area to volume ratio and mass fraction of each element in the material, as determined by bulk XRF analysis (Table 2).

3. Results and Discussion

3.1 Chabazite characterisation

Characterisation of the as-received and Cs-chabazite (Fig. 1) revealed that the phase assemblage constituents were: chabazite (powder diffraction file (PDF) #00-034-0137), K-feldspar matched to sanidine ($KAlSi_3O_8$, PDF #00-010-0357) and mica, matched to phlogopite ($KMg_3(AlSi_3O_{10})(OH)_2$, PDF #00-010-0495). Calcite ($CaCO_3$, PDF #00-005-0586) was also observed in the as-received chabazite (unwashed). It is likely that other alkali feldspars (albite, microcline, orthoclase and anorthite) were present in minor fractions but they could not be differentiated as they have similar diffraction patterns. Alkali feldspars exist as a ternary solid solution within volcanic rocks (which was the source of chabazite in this study [22]) and are typically comprised of albite ($NaAlSi_3O_8$), orthoclase ($KAlSi_3O_8$) and anorthite ($CaAl_2Si_2O_8$) [31]. With the exception of a reduced calcite contribution, no significant differences were observed in the phase assemblage between the as-received chabazite and the Cs-chabazite, which indicated that Cs was incorporated *via* exchange into the chabazite framework.

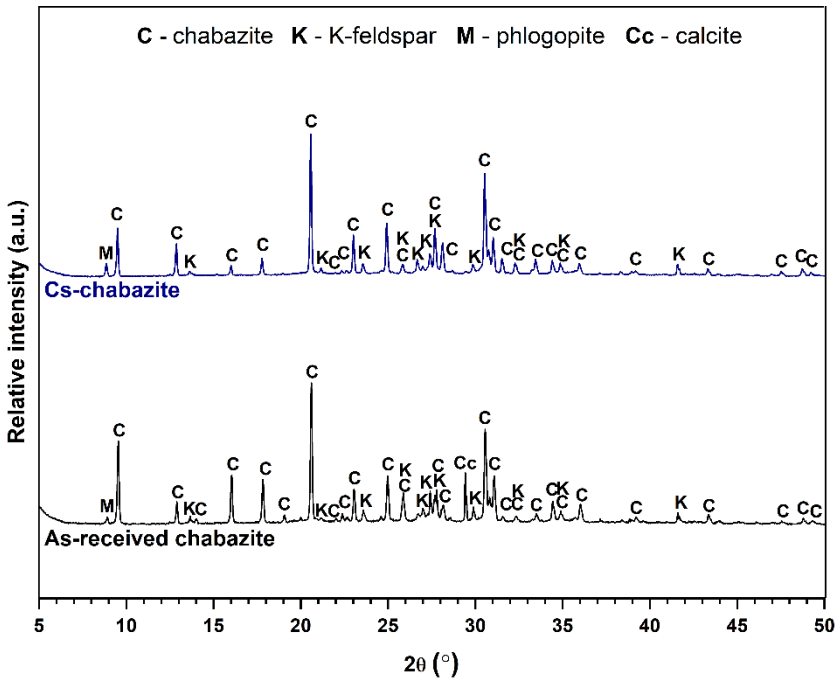

Figure 1. X-ray diffraction patterns of as-received chabazite and Cs-chabazite

193 The microstructures reported in Fig. 2 further demonstrates the heterogeneity of the natural chabazite.
194 The porous particles of various sizes were representative of chabazite, with strong elemental correlations
195 observed between Ca, K, Al and Si (Fig. 2A) with the addition of Cs in Fig. 2B (post exchange). The spherical
196 particles represent vitreous silica, which has a reported concentration of 18 wt. % in the as-received
197 chabazite [22]. The vitreous silica composition in the as-received chabazite was calculated by semi-
198 quantitative EDX analysis on an oxides basis as mol. % to be: 79.23 ± 2.48 SiO_2, 4.04 ± 0.94 Al_2O_3, 4.01 ±
199 0.88 CaO, 2.62 ± 0.39 K_2O, 1.21 ± 0.48 MgO and 0.26 ± 0.13 TiO_2 (the oxygen stoichiometry was assumed
200 on the basis of electroneutrality, due to the low accuracy of EDX for oxygen determination). This
201 composition is within the range of reported values for rhyolitic obsidian, which contains >66 mol. % SiO_2
202 [32]. Aluminosilicate particles rich in either Ca or K were also observed, which could represent anorthite
203 and K-feldspar (sanidine, orthoclase, microcline). To assess the potential for Cs incorporation in the
204 additional minor phases, K-feldspar (K), anorthite (Ca) and vitreous silica (O), EDX spectra of the as-
205 received chabazite and Cs-chabazite were compared in Fig. S1 (Supplementary Information). No distinct
206 signal could be detected for Cs (based on the $L\alpha_1$ emission at 4.285 keV) except for within the Cs-chabazite
207 grain, confirming Cs exchange within this phase, as shown in Fig. 2B.

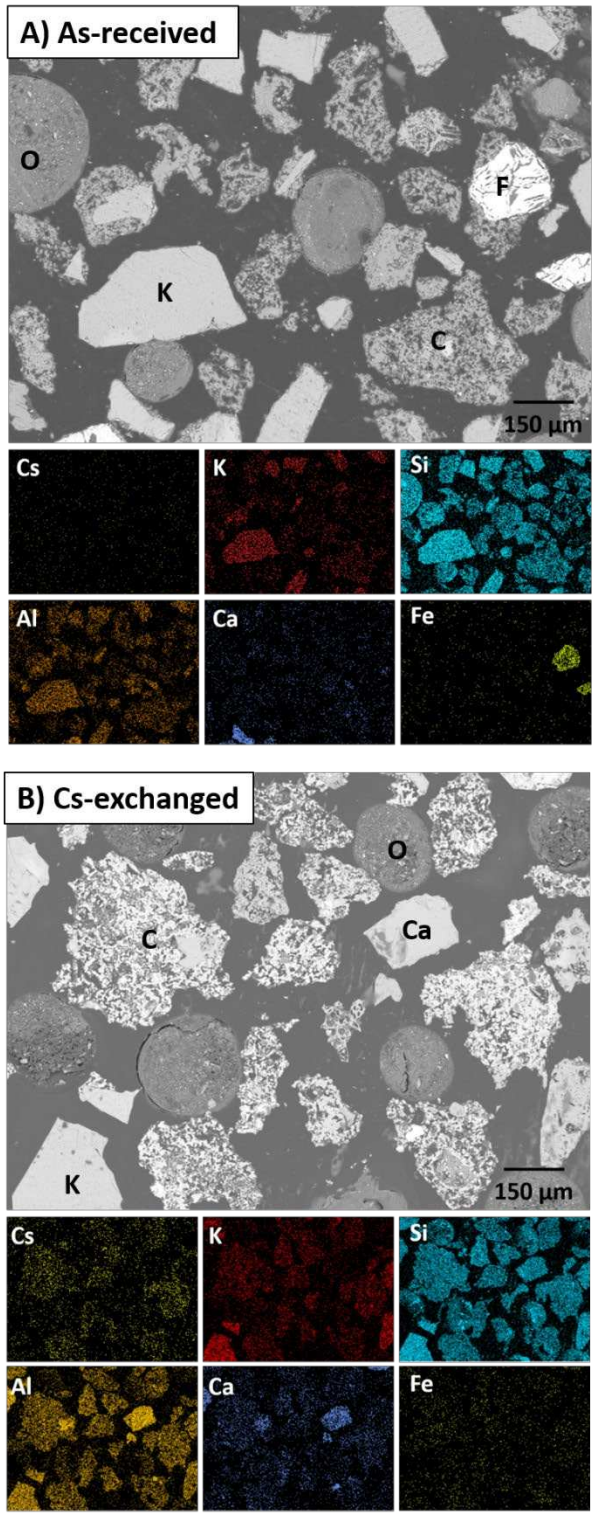

208

209 **Figure 2.** SEM/EDX of A) as-received chabazite and B) Cs-chabazite where labels indicate: C (chabazite), K

210 (K-feldspar), Ca (Ca-feldspar), O (vitreous silica) and F (iron oxide).

The dehydration behaviour of as-received chabazite (Fig. 3) revealed that the main mass loss occurred between 30-350 °C (equivalent to ~10%), which was determined by MS (Fig. 3B) to be associated with water desorption from the chabazite structure (nominally $(Na_2K_2CaMgAl_2Si_{12}O_{24}\cdot 6H_2O)$ and CO_2 from decomposition of accessory carbonate minerals. The main mass loss feature presented as two distinct but overlapping peaks centred at 178 °C and 232 °C (± 2 °C), which indicates that water was adsorbed on two sites within chabazite in accordance with the published crystal structure [33]. A second minor mass loss (~0.5%) was observed between 580-700 °C (centred at 636 ± 2 °C), which was associated with release of CO_2 from accessory carbonate minerals (Fig. 3B). The TGA/MS data were used to determine a suitable bake-out temperature during HIP canister preparation. Using Fig. 3, the pre-calcination and bake-out temperature was fixed to 300 °C, which would ensure that all water was removed from the sample whilst avoiding Cs volatisation, which should not occur below 400 °C [34].

The photographs in Fig. 4 show the HIP canister deformation after HIPing (for the 1250 °C/100 MPa sample). The internal volume was measured to decrease from 29.3 ± 1 cm^3 to 16.9 ± 0.8 cm^3, equivalent to an internal volume reduction of 42.5%. Post-HIP, each canister was sectioned to enable characterisation, which revealed that HIPing Cs-chabazite resulted in the formation of a dense monolith with no visible porosity but obvious heterogeneity across the sample, as evidenced by particles of varying colour within a black matrix (Fig. 4D). The conversion *via* HIPing of the highly dispersible Cs-chabazite granular particles (Fig. 4A) into a solid monolith is unmistakable in Figs. 4D-E, which clearly improved the passive safety of the material.

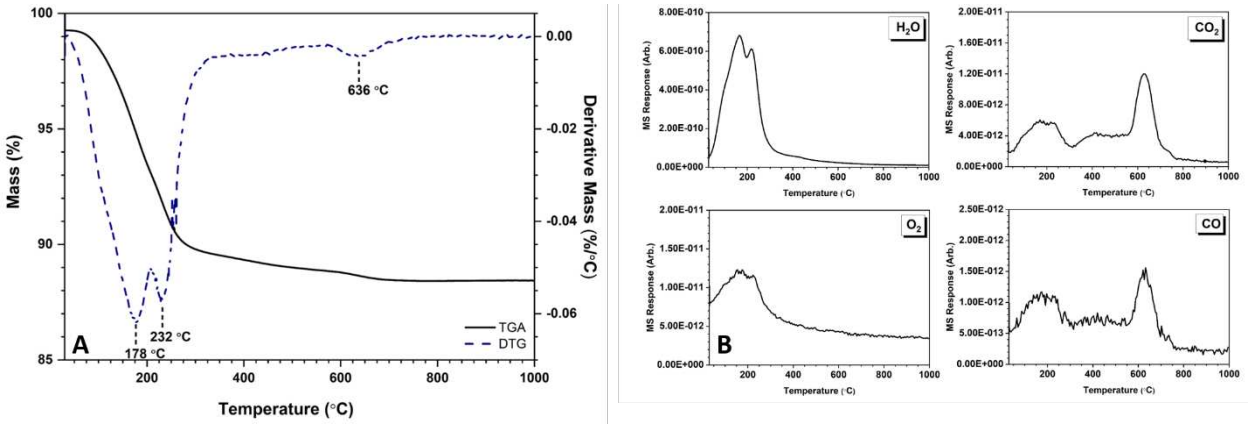

231

232 **Figure 3.** A) TGA/DTG thermograph and B) MS response of as-received chabazite up to 1000 °C.

233

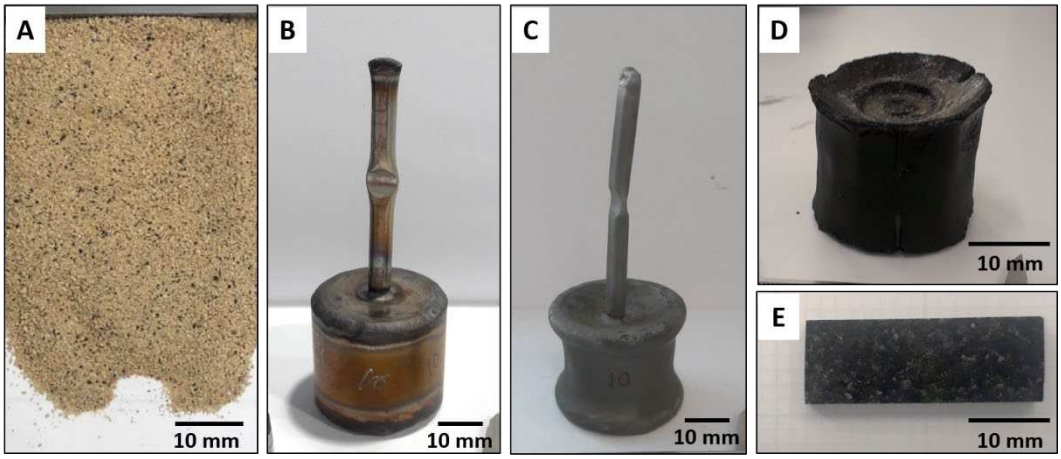

234

235 **Figure 4.** Photographs of 1250 °C/100 MPa Cs-chabazite, A) Cs-chabazite, B) prepared HIP canister (post
236 evacuation/bake-out), C) canister post-HIP, D) HIPed Cs-chabazite with canister removed and, E) a
237 polished section from D. Note: Photographs D-E are from a larger HIP can processed under the same
238 conditions, these images are shown to highlight the heterogeneity of the HIPed wasteform.

239

3.2 Characterisation of HIPed Cs-chabazite

In Figs. 5A-B, the XRD analysis revealed that the chabazite reflections identified in the pre-HIPed material (Fig. 2) were absent, indicative of a complete collapse of the chabazite framework, irrespective of the process conditions. At 1050 °C, the transformed phase assemblage could be described as a combination of framework feldspars, including: anorthite ($CaAl_2Si_2O_8$, PDF #00-041-1486); albite ($NaSi_3AlO_8$, PDF #00-010-393) and; leucite ($KAlSi_2O_6$, PDF #01-076-2298), with minor reflections attributed to diopside ($CaMgSi_2O_6$, PDF #01-075-1092). At 1150 °C, the relative intensities of all phases except leucite decreased, in a trend which continued up to 1250 °C, resulting in leucite being the dominant crystalline phase in HIPed Cs-chabazite. Diffuse scattering observed between $15° < 2\theta < 35°$ was noted to increase as the HIPing temperature increased, which is associated with the formation of a vitreous aluminosilicate phase; given the reduced relative intensity (or absence) of reflections associated with in anorthite, albite and diopside. As confirmed by EDX analysis, shown below, the glass phase likely has a composition rich in Ca, K, Na, Mg, Al and Si, consistent with vitrification of the aforementioned minerals. The XRD data revealed that a systematic change in the phase assemblage of HIPed Cs-chabazite when the temperature was varied, in materials processed under both 100 MPa and 50 MPa (Fig. 5B). Therefore, it is possible to conclude that the conversion of Cs-chabazite to a glass-ceramic by HIPing was controlled by the temperature regime rather than pressure. However, production of a satisfactory wasteform at a lower pressure of 50 MPa is preferable, from an operational safety perspective, to reduce risk to as low as reasonably practicable.

The K-feldspar identified after conversion of Cs-chabazite at all temperatures was the high-temperature polymorph, leucite ($KAlSi_2O_6$) with a cubic structure. This is somewhat unexpected since at temperatures of > 625 °C, leucite is known to undergo a tetragonal ($I4_1/a$) to cubic ($Ia\bar{3}d$) inversion [35, 36] but, on cooling, it should revert back to the tetragonal structure [37]. Since it was not possible to index any of the reflections to the cubic ($Ia\bar{3}d$) Cs-feldspar endmember pollucite ($CsAlSi_2O_6$) [38], a plausible explanation for the room temperature cubic structure could be Cs incorporation within the $KAlSi_2O_6$ lattice [39, 40]. The tetragonal and cubic structures of leucite can be differentiated by the cavity size in which the K^+ ion resides, with average K-O bond lengths of ~2.93-3.00 Å and 3.35-3.54 Å, respectively [36, 37]. Given that the ionic radius of Cs^+ is larger than that of K^+, incorporation of Cs^+ within the framework channels of leucite could prevent conversion to the lower symmetry structure on cooling. The Cs/K ratio within leucite will be considered further in the following discussion.

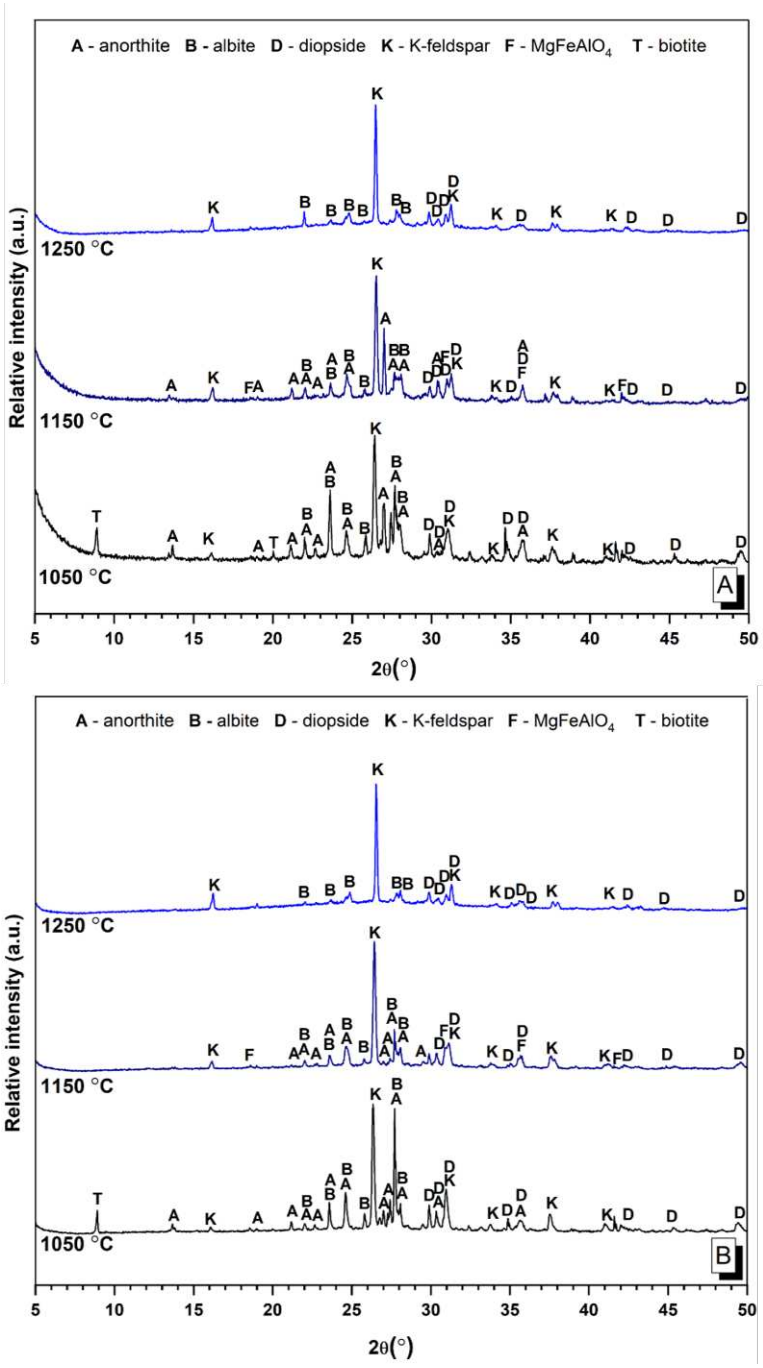

269

270 **Figure 5.** XRD patterns of Cs-chabazite HIPed between 1050-1250 °C and A) 100 MPa or B) 50 MPa

271 XRF analysis (Table 2) confirmed successful retention of Cs_2O was achieved *via* HIPing with an average of
272 2.50 wt. % measured across the three processing temperatures at 100 MPa. There was variability in the
273 measured Cs_2O content of the HIPed material, ranging from 2.33 to 2.73 wt. % (Table 2), which was

thought to be associated with the high heterogeneity of this material, resulting in slightly different feed composition and hence Cs_2O content. The Cs_2O retention was calculated to be 85% (mean), 80% (minimum; 1150 °C) and 95% (maximum; 1250 °C) when compared to Cs-chabazite feed (using Tables 1-2). Following HIP canister preparation (discussed in Section 2.1), the canisters were hermetically sealed prior to thermal treatment and thus, there is no expectation that Cs volatilisation would occur during successful HIP processing, irrespective of processing temperature (i.e. where successful represents consolidated canisters with no weld failures).

Table 2. XRF spectroscopy of HIPed Cs-chabazite at varying temperatures (wt. %), errors indicated in parenthesis

Oxide	1050 °C	1150 °C	1250 °C
Al_2O_3	20.07 (± 0.13)	20.27 (± 0.16)	20.64 (± 0.11)
CaO	6.25 (± 0.01)	6.04 (± 0.02)	5.62 (± 0.06)
Cs_2O	2.45 (± 0.07)	2.33 (± 0.03)	2.73 (± 0.03)
Fe_2O_3	6.43 (± 0.15)	5.67 (± 0.19)	4.59 (± 0.09)
K_2O	6.85 (± 0.08)	7.11 (± 0.09)	7.03 (± 0.04)
MgO	2.12 (± 0.01)	2.12 (± 0.01)	1.77 (± 0.02)
Na_2O	0.75 (± 0.01)	0.80 (± 0.02)	0.80 (± 0.04)
SiO_2	53.93 (± 0.24)	54.57 (± 0.36)	55.67 (± 0.37)
TiO_2	0.75 (± 0.02)	0.70 (± 0.03)	0.63 (± 0.02)
Density (g/cm^3)	2.7226 (± 0.0036)	2.6639 (± 0.0024)	2.6489 (± 0.0016)

The microstructure of HIPed Cs-chabazite (Figs. 6-7) confirmed the presence of a multi-phase glass-ceramic composite at all temperatures and pressures investigated. The proportion of the glass fraction in the HIPed wasteform appeared to increase with increasing processing temperature from 1050 to 1250 °C, which is attributed to a reduction in phases containing Ca, Mg, Al and Si, identified by XRD as anorthite, albite and diopside minerals. The bright grains, interspersed throughout the glass matrix, were rich in Cs, K, Al and Si, and represent cubic Cs/K-leucite as identified in Fig 5. At 1050 °C, there was also evidence for a K-feldspar with no Cs incorporation (Fig. 6A, centre bottom); which is likely present as a trace component

292 from the starting material (sanidine; $KAlSi_3O_8$) that was not detectable in the XRD data due to complex
293 diffraction patterns. At 1150 °C under both the 100 and 50 MPa regimes (Figs. 6B and 7B), the formation
294 of a spinel phase (rich in Mg and Fe) was observed, indicating that its formation is temperature dependent
295 over a narrow range. At 1250 °C (both pressures; Figs. 6C and 7C), the microstructure agreed with the XRD
296 (Fig. 5) where a reduction in the overall phase heterogeneity was observed in favour for a Cs-rich phase
297 (bright areas) and a Cs-deficient (mid-grey) phase, which were assigned to Cs/K-leucite and a glassy phase,
298 respectively. The SEM/EDX data revealed that the microstructure was independent of the pressure
299 imposed on the system, in agreement with the XRD results and, furthermore, that tailored microstructures
300 could be achieved *via* HIPing.

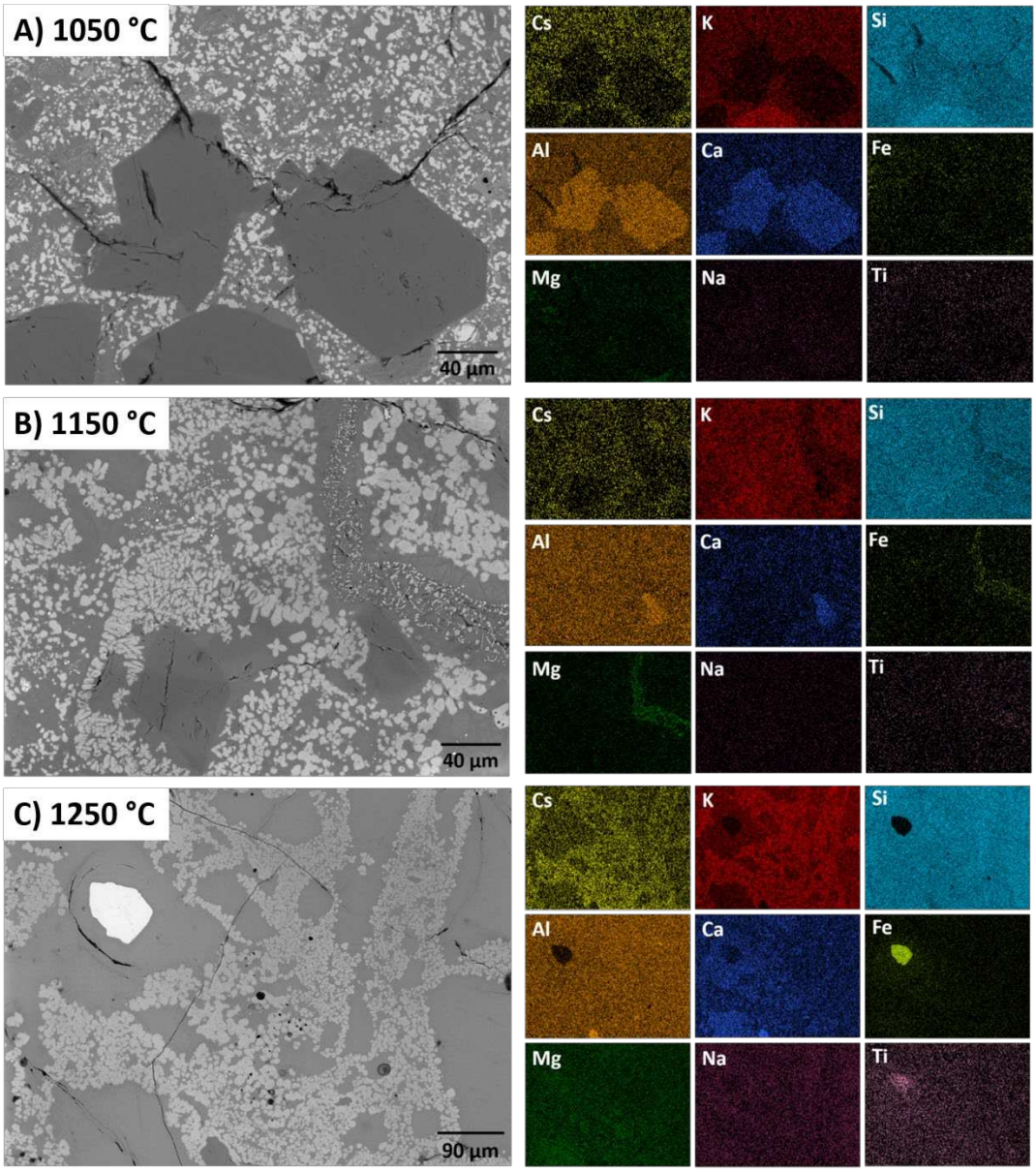

Figure 6. SEM/EDX of Cs-chabazite HIPed between 1050-1250 °C at 100 MPa

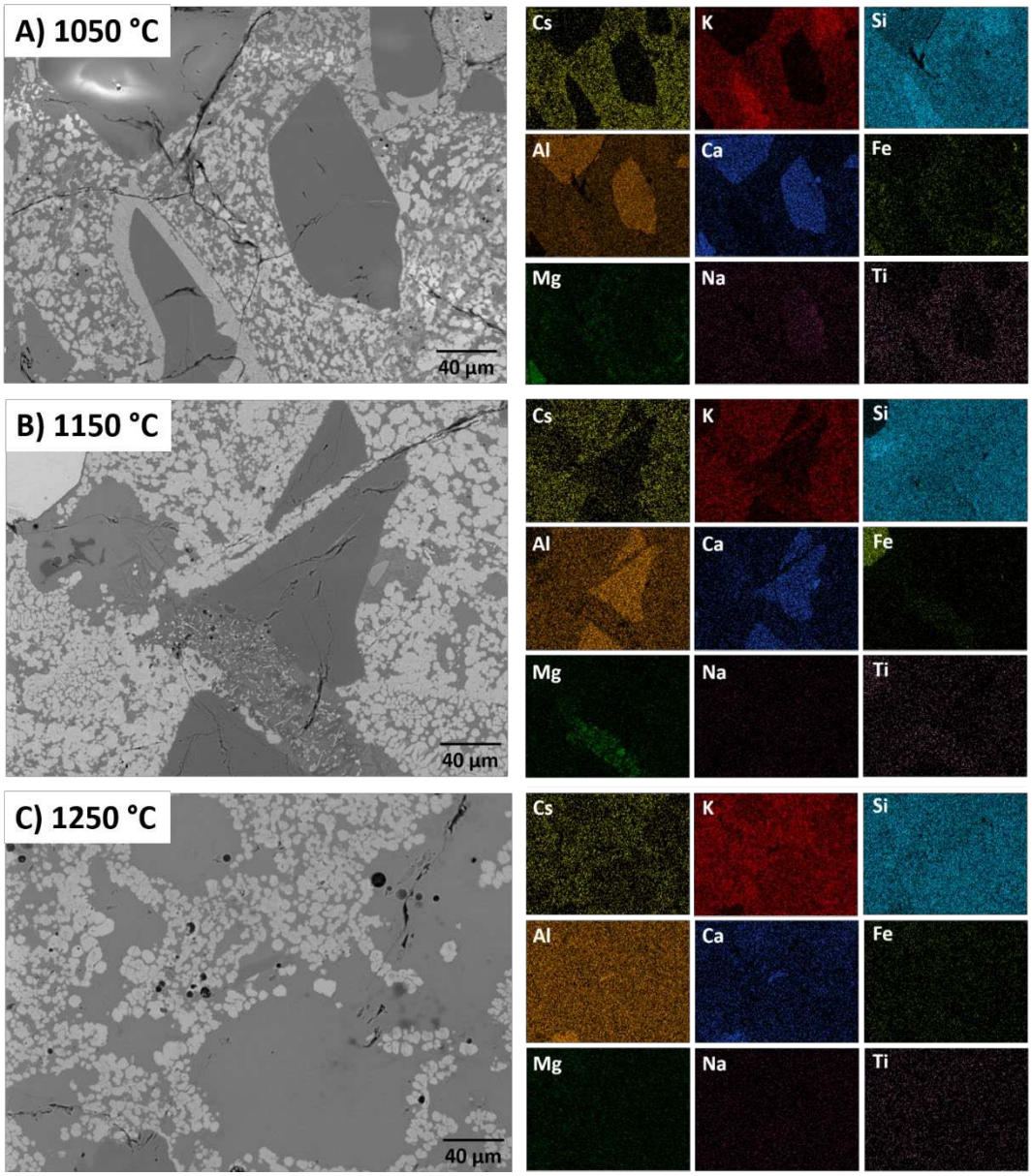

303

304 **Figure 7.** SEM/EDX of Cs-chabazite HIPed between 1050-1250 °C at 50 MPa

305

306 To evaluate the partitioning of Cs between the ceramic and glass phase, semi-quantitative EDX analysis
307 was performed on Cs-chabazite HIPed at 1250 °C and 100 MPa (Fig. 8). The calculated composition was
308 based on the average of 10 spot analyses per phase and are reported to one standard deviation (Table 3).
309 The crystallites were determined to have a composition of $Cs_{0.15(3)}K_{0.57(4)}Al_{0.90(4)}Si_{2.24(5)}O_6$ (herein referred

to as Cs/K-feldspar). Compared to the typical feldspar composition of $MAlSi_2O_6$ (where M represents alkali metals), this phase is Si-rich and Al/alkali metal-deficient. The Al/Si ratio for leucite feldspar should be 0.5 whereas, in this study, an Al/Si ratio of 0.32 ± 0.10 (Table 3) was achieved. The elemental Cs/K ratio was 0.25:1, with the total alkali metal content of the feldspar calculated to be 11.39 ± 1.10 mol. %. The Cs/K-feldspar was incorporated within a K_2O-CaO-MgO-Al_2O_3-SiO_2 (alkali alkaline earth aluminosilicate) glass with a high SiO_2 content and an Al/Si ratio of ~1:12. This contained 0.71 ± 0.17 mol. % Cs_2O, which is equivalent to 23% of the measured Cs_2O inventory within the wasteform (Table 3). Based on these results, it is possible to state that Cs preferentially partitioned into crystalline phases, however, a lower concentration also partitioned into the vitreous phase.

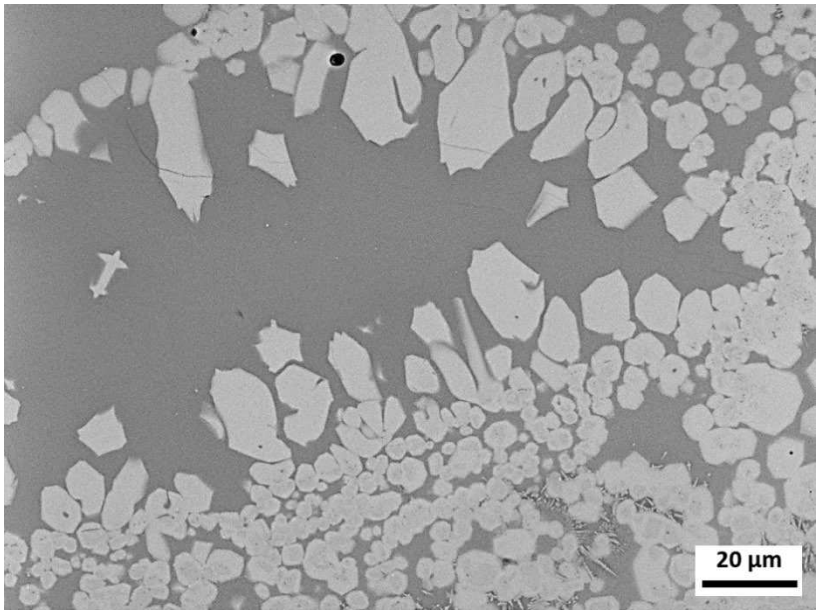

Figure 8. BSE micrograph of Cs-chabazite HIPed at 1250 °C/100 MPa used for compositional analysis, showing crystallites of Cs-containing leucite distributed within a glass matrix.

Table 3. Semi-quantitative EDX analysis of the 1250 °C/100 MPa HIPed chabazite in Figure 8 (errors indicated in parenthesis)

Oxide mol. %	Feldspar	Glass
Al_2O_3	14.27 (± 0.61)	11.62 (± 0.71)
CaO	1.41 (± 0.79)	7.53 (± 1.37)
Cs_2O	2.40 (± 0.43)	0.71 (± 0.17)
Fe_2O_3	1.07 (± 0.30)	1.24 (± 0.58)
K_2O	8.99 (± 0.67)	6.11 (± 0.89)
MgO	0.81 (± 0.47)	1.81 (± 0.78)
Na_2O	0.00 (± 0.00)	0.21 (± 0.21)
SiO_2	71.06 (± 1.64)	70.77 (± 2.12)
Element at. %	**Feldspar**	**Glass**
Al/Si	0.40 (± 0.02)	0.33 (± 0.01)
Cs+K/Si	0.32 (± 0.02)	0.19 (± 0.03)
Cs+K/Al	0.80 (± 0.07)	0.57 (± 0.08)
Cs/K	0.25 (± 0.05)	0.12 (± 0.02)

3.3 Durability Assessment

PCT-B durability studies, to evaluate the performance of Cs-chabazite wasteforms, were conducted according to ASTM standard C1285-14 [30] up to 28 days for samples fabricated at 1050-1250 °C and 100 MPa. The pH and elemental normalised mass loss (NL_i) values are presented in Fig. 9. All HIPed Cs-chabazite wasteforms had a relatively low pH throughout the duration of the experiment, which ranged between pH 8.6-8.7 ± 0.3 (1050 °C) and 7.8-8.2 ± 0.2 (1250 °C), with the 1050 °C samples consistently achieving a higher pH than the wasteforms processed at higher temperatures (Table 4). These values are lower than high level waste (HLW) glasses under similar conditions, consistent with the relatively low alkali and alkaline earth content of the aluminosilicate glass network. In compositions where the Si content is >67 mol. %, there are fewer interconnected non-bridging Si-O bonds, which provide dissolution pathways [41]. Therefore, the glass produced at 1250 °C (SiO_2 at 70.77 ± 2.12 mol. %; Table 3) has the potential to supress ion migration and reduce dissolution (and thus, stabilise a low pH) leading to improved durability performance.

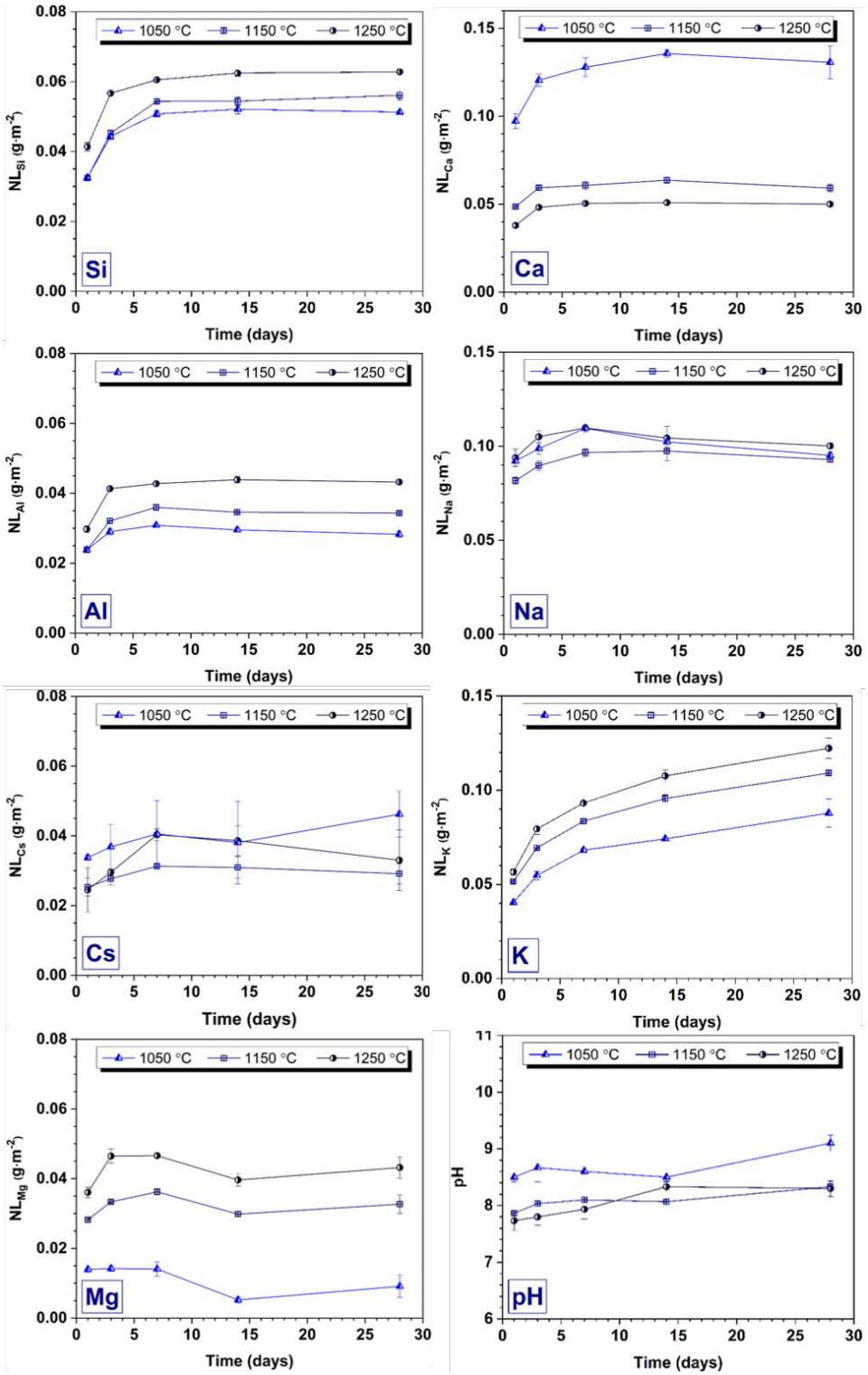

Figure 9. Normalised elemental mass loss for Cs-chabazite HIPed between 1050-1250 °C/100 MPa

The general trend for the Cs-chabazite wasteforms followed the typical behaviour of HLW waste glasses, with a rapid elemental release (initial regime, 1-7 d) followed by a rate drop and attainment of pseudo-steady state (residual regime, 7-28 d) for NL_{Si}, NL_{Al} and NL_{Ca}. Whilst the trend was similar, HLW glass dissolution occurs congruently, which cannot be assumed (nor expected) in this study due to the presence of mixed crystalline and vitreous phases. For NL_{Mg}, the elemental release decreased at 14 d, which is also commonly observed for Mg-bearing HLW glasses (e.g. UK MW glass). Mg will readily scavenge Si to form secondary phyllosilicate phases, often with a drop in pH and promotion of glass dissolution [42-44]. However, in conditions where the pH ≤ 8, the precipitation of Mg-bearing phyllosilicates is reduced and in-turn, this decreases the rate of glass alteration [44], which could be ascribed to the relatively low NL_{Si} values.

For almost all elements (Fig. 9) the effect of processing temperature was the same, where a higher processing temperature resulted in higher elemental release (*i.e.* 1250 °C > 1150 °C > 1050 °C). By SEM analysis, the glass fraction was observed to increase commensurately with processing temperature (in agreement with XRD data. Therefore, the higher elemental release at 1250 °C indicates the glass phase is more soluble than the crystalline phase (Cs/K-feldspar), as evidenced in Figs. S2-S7. The incongruent dissolution of the HIPed Cs-chabazite wasteforms (at all temperatures) can be understood by exploring the NL_{Cs} and NL_K relationship. Cs and K are inextricably linked in the crystalline phase (Cs/K-feldspar) and both have similar ΔG_{hyd} of Cs^+ (-250 kJ mol^{-1}) and K^+ (-295 kJ mol^{-1}) [45]. This suggests that if the Cs/K-feldspar was dissolving, NL_{Cs} and NL_K should follow the same trend, however, unlike NL_{Cs}, there was no steady-state achieved for NL_K (Fig. 9) but rather continued elemental release. This dissimilarity in NL_{Cs} and NL_K must therefore arise from the distribution of these elements across the crystalline and glass phases, where Cs favoured the more durable crystalline phase compared to K (Table 3), which was distributed between both the crystalline and less durable glass phase. This concurs with a recent study that compared the dissolution behaviour of a crystalline feldspar ($Na_{0.83}K_{0.02}Ca_{0.07}Al_{1.06}Si_{2.96}O_8$) and a glass of the same chemical composition, which ascertained that the glass phase dissolved more rapidly (up to 10-20 times faster at pH 10) than the crystalline feldspar [46]. This difference was attributed to the local atomic structure of the material, with the open structure of the glass encouraging ion exchange between water and alkali elements whilst such diffusion related phenomenon were not observed in the crystalline material [46].

An exception to the trend where elemental release is higher commensurate with processing temperature, was Ca. The highest Ca release was observed for the material processed at 1050 °C, in which the majority of the Ca was located within anorthite and diopside as distinct grains within the bulk matrix (based on SEM/EDX; Fig. 6), whereas at 1250 °C, no such features were identified. Whilst for NL_{Cs}, there was no clear trend associated with the processing temperature or Cs_2O concentration (Table 2). This was attributed to relatively low NL_{Cs} values (consistent with Cs preferentially partitioned in the durable crystalline phase), which were within one or two standard deviations at each time point. This close relationship was dissimilar to all other elements where there was a clear separation between the processing temperatures (and error bars) allowing for trends to be observed.

Examination of the HIPed Cs-chabazite grains at 28 d post dissolution (Figs S2-S7) revealed cracking damage evident on the periphery of the glassy portions of grains, while the crystalline regions remained largely intact, confirming the hypothesis that the glass dissolved preferentially. At all temperatures, no evidence of the formation of secondary minerals resulting from dissolution was found. A silica gel layer, containing Si and Al, responsible for the observed "rate drop" was apparent at the surface of some grains (e.g. Fig. S5), although it was not possible to undertake a detailed analysis of its composition at the resolution employed. Future investigation using direct surface retreat rate observation, e.g. vertical scanning interferometry (VSI), could be utilised to elucidate and define the contribution of each component phase present in the HIPed Cs-chabazite to the overall dissolution.

Table 4. Dissolution rates of HIPed Cs-chabazite at varying temperatures during the $NL_{i,initial}$ (1-7 d) and $NL_{i,residual}$ (7-28 d) regimes

Sample	Day	Av. pH	Na (g m^{-2} d^{-1})	Si (g m^{-2} d^{-1})	Cs (g m^{-2} d^{-1})
1050	1-7	8.6 ± 0.2	(2.87 ± 0.12) x 10^{-3}	(3.24 ± 0.92) x 10^{-3}	(1.21 ± 0.16) x 10^{-3}
1150	1-7	8.0 ± 0.1	(2.43 ± 0.49) x 10^{-3}	(3.41 ± 0.82) x 10^{-3}	(0.95 ± 0.05) x 10^{-3}
1250	1-7	7.8 ± 0.2	(1.96 ± 0.79) x 10^{-3}	(1.15 ± 0.68) x 10^{-3}	(2.69 ± 0.03) x 10^{-3}
1050	7-28	8.7 ± 0.3	(6.63 ± 0.95) x 10^{-4}	(0.13 ± 0.34) x 10^{-4}	(3.21 ± 1.70) x 10^{-4}
1150	7-28	8.2 ± 0.1	(1.85 ± 0.45) x 10^{-4}	(0.78 ± 0.26) x 10^{-4}	(0.99 ± 0.15) x 10^{-4}
1250	7-28	8.2 ± 0.2	(4.55 ± 0.31) x 10^{-4}	(1.10 ± 0.21) x 10^{-4}	(3.18 ± 0.52) x 10^{-4}

The normalised dissolution rates (NR_i) quantified by linear regression for the $NR_{i,initial}$ and $NR_{i,residual}$ regimes are shown in Table 4. The initial Na release rate, $NR_{Na,initial}$, determined for the material produced at 1050 °C, (2.87 ± 0.12) x 10^{-3} g m^{-2} d^{-1}, was marginally higher than for the material produced 1250 °C, (1.96 ± 0.79) x 10^{-3} g m^{-2} d^{-1}. It was demonstrated (Table 3) that Na was exclusively located in the vitreous phase at 1250 °C, and, as such, supports the conclusion that alkali alkaline earth aluminosilicate glass underwent dissolution in this study. The residual rates of Na release, $NR_{Na,residual}$, were reduced by an order of magnitude compared to the initial rates , following the rate drop at > 7 d. In HLW (UK MW with 25 wt. % waste loading), the NR_{Na} at 90 °C and pH 8 was (1.583 ± 0.209) g m^{-2} d^{-1}, which increased to (1.91 ± 0.25) g m^{-2} d^{-1} at a higher waste loading (30 wt. % MW glass) [47]. Whilst in an ILW glass wasteform proposed for Mg-rich wastes, the NR_{Na} was observed to be (2.62 ± 0.45) x 10^{-2} g m^{-2} d^{-1} and (4.06 ± 0.16) x 10^{-3} g m^{-2} d^{-1} in the initial and residual regimes, respectively [48]. The NR_{Na} values in the current study where at least an order of magnitude lower than both the HLW and ILW proposed glass wasteforms, demonstrating that these HIPed wasteforms have an improved performance compared to vitrified wasteforms intended for geological disposal in the UK, at least in short term experiments designed to assess the inherent material dissolution rate. Nevertheless, further investigation is warranted to examine the long term dissolution behaviour of this composite vitreous wasteform and the potential for rate resumption.

Since there are few studies related to the durability of thermally treated chabazite spent ion exchange material, we compare the results from the present study with those from thermally-treated Cs-exchanged clinoptilolite ($(Na,K,Ca)_{2\text{-}3}Al_3(Al,Si)_2Si_{13}O_{36}{\cdot}12H_2O$), which is also a natural zeolite-based aluminosilicate framework mineral used in radionuclide water treatment. The thermal treatment of Cs-clinoptilolite (containing ~1 wt. % Cs_2O) *via* HIPing (1200 °C, 100 MPa) was achieved with 5 wt. % addition of glass additives (sodium aluminate or borax) [29]. The chemical durability assessment was performed under almost identical conditions as those used in the current investigation (SA/V, T, *t* and solution) with the NL_{Cs} reported to be (4.91 and 6.79) x 10^{-4} g m^{-2} d^{-1}after 28 days for the sodium aluminate and borax modified compositions, respectively [29]. In the current study, the overall normalised release rate for Cs (1-28 d) was calculated to be (8.69 ± 0.62) x 10^{-5} g m^{-2} d^{-1}at 1250 °C, an order of magnitude better than HIPed Cs-clinoptilolite, with respect to Cs release.

Whilst the full Cs-feldspar endmember (pollucite, $CsAlSi_2O_6$) was not attained (nor targeted) in this study, Cs incorporation into feldspars has been investigated as an immobilisation matrix for radiocaesium at the

Hanford site, USA [49]. Pollucite, which can contain up 34 wt. % Cs_2O [50], was found to be a suitable candidate for ^{137}Cs due to its high durability, low solubility and thermal stability [49], and has been suggested as an appropriate immobilisation matrix for ^{137}Cs [49, 51-53]. For example, under hydrothermal conditions (200 °C/30 MPa for 4 weeks), the measured release of Cs from pollucite was just 0.04% in deionised water [54]. Therefore, it is plausible that the formation $Cs_{0.15(3)}$ of $K_{0.57(4)}Al_{0.90(4)}Si_{2.24(5)}O_6$ feldspar (composition formed by processing at 1250 °C/100 MPa) could provide a durable host matrix for radiocaesium, in addition to the HIP process itself minimising the risk of Cs volatisation and secondary waste generation. Overall, the elemental release rates were low throughout the duration of this study and at all processing temperatures, which indicates that the hot isostatic pressing of spent ion exchange materials can lead to the formation of durable glass-ceramic wasteforms.

4. Conclusions

The passive safety of spent ion exchange materials was improved by conversion into a chemically and physically stable monolith wasteform by thermal treatment of Cs-chabazite *via* HIPing. A multi-phase glass-ceramic with a high Cs retention was achieved at 1050, 1150 and 1250 °C under two pressure regimes. Characterisation of HIPed wasteforms by XRD and SEM/EDX revealed the complete collapse of the chabazite framework structure at all temperatures, with the processing temperature observed to control the phase assemblage. At 1250 °C, a Cs/K-leucite was formed which contained 77 % of the total Cs_2O inventory, with the remaining fraction (23%) located within an alkali alkaline earth aluminosilicate glass (K_2O-CaO-Mgo-Al_2O_3-SiO_2). The normalised Na release rates were observed to be an order of magnitude lower than values reported HLW and ILW glasses, whilst the Cs release rate remained low for the duration of the experiment at all temperatures, which was thought to be released preferentially from the glass fraction rather than the Cs/K-feldspar.

For Cs-loaded ion exchange materials, the radiological risk will be significantly reduced within ~300 years (Cs^{137} $t_{1/2}$ = 30.2 years) without any engineering imposed on the waste. Therefore, the fact that these HIPed Cs-chabazite wasteforms perform (up to day 28) better than or comparable to reported values for HLW glasses (with a longer required service life for long-lived radionuclides) is a good indication that HIPing would be suitable treatment method for spent ion exchange materials. However, additional data

is required at extensive time periods (months to years) to determine the long-term durability of Cs-chabazite, with particular emphasis on larger-scale wasteforms (*i.e.* greater than 35 g) to support potential scale-up operations. Future work should investigate the impact of chlorine incorporation within Cs-chabazite on the wasteform phase assemblage and interaction with the HIP canister (sea water was used at Fukushima Daiichi NPP for emergency cooling the damaged reactors) [55].

Overall, this study demonstrated the efficacy of HIPing to convert inorganic ion exchange materials into durable glass-ceramic wasteforms in addition to a notable volume reduction and a relatively high waste loading (70 wt. %). HIPing was shown to be a suitable thermal treatment technology with respect to increasing the passive safety of conditioned spent ion exchange materials, whilst also reducing the risk associated with loss of containment of these stored wastes. This study focussed specifically on the waste management for Fukushima Daiichi NPP, however, the thermal treatment of spent ion exchange materials *via* HIPing could successfully be applied on a wider scale to all sites where these types of inorganic wastes are generated.

Supplementary Information

Additional SEM/EDX data of as-received chabazite, Cs-chabazite and HIPed Cs-chabazite (post-dissolution)

ACKNOWLEDGMENTS

The authors are grateful to UKRI EPSRC for sponsorship of this research under grant references EP/N017617/1, EP/P013600/1, EP/S01019X/1 and EP/S032959/1. CLC is grateful to the University of Sheffield for the award of a Vice Chancellor's fellowship and EPSRC for the award of an Early Career Fellowship under grant reference EP/N017374/1. This research utilised the HADES/MIDAS facility and Henry Royce Institute at the University of Sheffield established with financial support from UKRI EPSRC and BEIS, under grant EP/T011424/1 and EP/P02470X/1 [56]. We are grateful to the eight anonymous reviewers for their careful consideration of our draft manuscript and suggestions for improvement.

Competing interest statement

The authors declare that they have no known competing financial interests or personal relationships that could have appeared to influence the work reported in this paper.

REFERENCES

[1] Tokyo Electric Power Company, Fukushima nuclear accident analysis report, in, Tokyo Electric Power Company Holdings, Inc., Toyko, Japan, , 2012.

[2] International Atomic Energy Agency, The Fukushima Daiichi accident. Technical Volume 1: Description and context of the accident, in, International Atomic Energy Agency, Vienna, Austria, 2015.

[3] J. Lehto, R. Koivula, H. Leinonen, E. Tusa, R. Harjula, Removal of Radionuclides from Fukushima Daiichi Waste Effluents, Separation & Purification Reviews, 48 (2019) 122-142.

[4] D. Delacroix, J. P. Guerre, P. Leblanc, C. Hickman, Radionuclide and radiation protection data handbook 2002, Radiation Protection Dosimetry, Nuclear Technology Publishing, 98 (2002) 1-168.

[5] M.S. Denton, J.L. Mertz, W.D. Bostick, Fukushima nuclear crisis recovery: a modular water treatment system deployed in seven weeks, in: Waste Management, AZ, USA, 2012.

[6] UOP, IONSIV^{TM} selective media: water decontamination at Japan's Fukushima Daiichi nuclear power plant, in, UOP LLC, USA, September 2013.

[7] Tokyo Electric Power Company, Situation of storage and treatement of accumulated water including highly concencentrated radioactive materials and Fukushima Daiichi nuclear power station (448th release) - April 20, 2020, in, Tokyo Electric Power Company Holdings, Inc, Toyko, Japan, 2020.

[8] I. Yamagishi, R. Nagaishi, C. Kato, K. Morita, A. Terada, Y. Kamiji, R. Hino, H. Sato, K. Nishihara, Y. Tsubata, S. Tashiro, R. Saito, T. Satoh, J. Nakano, W. Ji, H. Fukushima, S. Sato, M. Denton, Characterization and storage of radioactive zeolite waste, Journal of Nuclear Science and Technology, 51 (2014) 1044-1053.

[9] H.V. Atkinson, S. Davies, Fundamental aspects of hot isostatic pressing: an overview, Metallurgical and Materials Transactions A, 31A (2000) 2981-3000.

[10] P.G. Heath, Stewart, Martin W. A., Moricca, Sam. Hyatt, Neil C., Hot-isostatically pressed wasteforms for Magnox sludge immobilisation, Journal of Nuclear Materials, 499 (2018) 233-241.

[11] L.J. Gardner, Walling, S. A., Hyatt, N. C., Hot isostatic pressing: thermal treatment trials of inactive and radioactive simulant UK intermediate level waste, IOP Conference Series: Materials Science and Engineering, 818 (2020) 012009.

[12] K.J. Bateman, E.P. Hart, W.M. McCartin, D.L. Wahlquist, Summary of calcine disposal development using hot isostatic pressing, in, Idaho National Laboratory, Idaho, USA, 2013.

[13] E.R. Vance, M.W.A. Stewart, S.A. Moricca, Progress at ANSTO on SYNROC, Journal of the Australian Ceramic Society, 50 (2014) 38-48.

[14] S.M. Thornber, P.G. Heath, G.P. Da Costa, M.C. Stennett, N.C. Hyatt, The effect of pre-treatment parameters on the quality of glass-ceramic wasteforms for plutonium immobilisation, consolidated by hot isostatic pressing, Journal of Nuclear Materials, 485 (2017) 253-261.

[15] Nuclear Decommissioing Authority, Progress on plutonium consolidation, storage and disposition in, 2019.

[16] L.R. Blackburn, L.J. Gardner, S.K. Sun, E.R. Maddrell, M.C. Stennett, C.L. Corkhill, N.C. Hyatt, Hot Isostatically Pressed Zirconolite Wasteforms for Actinide Immobilisation, IOP Conference Series: Materials Science and Engineering, 818 (2020) 012010.

[17] S.M. Thornber, L.M. Mottram, A.R. Mason, P. Thompson, M.C. Stennett, N.C. Hyatt, Solubility, speciation and local environment of chlorine in zirconolite glass–ceramics for the immobilisation of plutonium residues, RSC Advances, 10 (2020) 32497-32510.

[18] M.W.A. Stewart, S.A. Moricca, T. Eddowes, Y. Zhang, E.R. Vance, G.R. Lumpkin, M.L. Carter, M. Dowson, M. James, The use of hot-isostatic pressing to process nuclear waste forms, in: Proceedings of the 2009 12th International Conference on Environmental Remediation and Radioactive Waste Management ICEM2009, Liverpool, UK, 2009, pp. ICEM2009-16253.

[19] E.R. Vance, S. Moricca, B.D. Begg, M.W.A. Stewart, Y. Zhang, M.L. Carter, Advantages hot isostatically pressed ceramic and glass-ceramic waste forms bring to the immobilization of challenging intermediate- and high-level nuclear wastes, Advances in Science and Technology, 73 (2011) 130-135.

[20] D.J. Gregg, Farzana, Rifat, Dayal, Pranesh, Holmes, Rohan, Triani, Gerry, Synroc technology: Perspectives and current status (Review), Journal of the American Ceramic Society, 00 (2020) 1-18.

[21] Nuclear Decommissioing Authority, NDA plutonium topic strategy: Credible option techincal analysis. SAF/081208/006/02, in, Nuclear Decommissioing Authority, 2009.

[22] Verdi S.p.A, Zeover data sheet, in, Verdi S.p.A, Torrino, Italy, 2015.

[23] D. Pletser, R.K. Chinnam, M. Kamoshida, W.E. Lee, Immobilisation process for contaminated zeolitic ion exchangers from Fukushima, MRS Advances, 1 (2016) 4089-4094.

[24] R.M. Barrer, J.A. Davies, L.V.C. Rees, Thermodynamics and thermochemistry of cation exchange in chabazite, Journal of Inorganic and Nuclear Chemistry, 31 (1969) 219-232.

[25] M. Kong, Z. Liu, T. Vogt, Y. Lee, Chabazite structures with Li^+, Na^+, Ag^+, K^+, NH_4^+, Rb^+ and Cs^+ as extra-framework cations, Microporous and Mesoporous Materials, 221 (2016) 253-263.

[26] D. Wahlquist, K. Bateman, T. Malewitz, Remote Sealing of Canisters for Hot Isostatic Pressing, in: ASME 2014 International Mechanical Engineering Congress and Exposition, 2014.

[27] R. Kimura, Y. Inagaki, K. Idemitsu, T. Arima, Vitrification processes of simulated cesium sorbing zeolite waste, Progress in Nuclear Energy, 108 (2018) 497-502.

[28] T.-Y. Chen, E.R. Maddrell, N.C. Hyatt, A.S. Gandy, M.C. Stennett, J.A. Hriljac, Transformation of Cs-IONSIV® into a ceramic wasteform by hot isostatic pressing, Journal of Nuclear Materials, 498 (2018) 33-43.

[29] P.G. Heath, Alternative procesing methods for the thermal treatment of radioactive wastes, in: Materials Science and Engineering, Univeristy of Sheffield, 2015.

[30] ASTM International, C1285-14 Standard Test Methods for Determining Chemical Durability of Nuclear, Hazardous, and Mixed Waste Glasses and Multiphase Glass Ceramics: The Product Consistency Test (PCT), in, West Conshohocken, PA, 2014.

[31] W.A.F. Deer, R.A. Howie, J. Zussman, An Introduction to the Rock-Forming Minerals, in, Mineralogical Society of Great Britain and Ireland, 2013.

[32] J.E. Ericson, A. Makishima, J.D. Mackenzie, R. Berger, Chemical and physical properties of obsidian: a naturally occuring glass, Journal of Non-Crystalline Solids, 17 (1975) 129-142.

[33] J.L. Stakebake, Characterization of natural chabazite and 5A synthetic zeolites: Part I. Thermal and outgassing properties, Journal of Colloid and Interface Science, 99 (1984) 41-49.

[34] M.I. Ojovan, W.E. Lee, An introduction to nuclear waste immobilisation - 2nd edition, 2 ed., Elsevier, Oxford, UK, 2013.

[35] K. Hirao, N. Soga, M. Kunugi, Thermal expansion and structure of leucite-type compounds, The Journal of Physical Chemistry, 80 (1976) 1612-1616.

[36] F. Mazzi, The crystal structure of tetragonal leucite, American Mineralogist, 61 (1976) 108-115.

[37] C. Palmer David, T. Dove Martin, M. Ibberson Richard, M. Powell Brian, Structural behavior, crystal chemistry, and phase transitions in substituted leucite: High-resolution neutron powder diffraction studies, in: American Mineralogist, 1997, pp. 16.

[38] D. Taylor, C.M.B. Henderson, The thermal expansion of the leucite group of minerals, American Mineralogist, 53 (1968) 1476-1489.

[39] P. He, Z. Yang, J. Yang, X. Duan, D. Jia, S. Wang, Y. Zhou, Y. Wang, P. Zhang, Preparation of fully stabilized cubic-leucite composite through heat-treating Cs-substituted K-geopolymer composite at high temperatures, Composites Science and Technology, 107 (2015) 44-53.

[40] P. He, D. Jia, M. Wang, Y. Zhou, Effect of cesium substitution on the thermal evolution and ceramics formation of potassium-based geopolymer, Ceramics International, 36 (2010) 2395-2400.

[41] C.M. Jantzen, K.G. Brown, J.B. Pickett, Durable Glass for Thousands of Years, International Journal of Applied Glass Science, 1 (2010) 38-62.

[42] B.M.J. Thien, N. Godon, A. Ballestero, S. Gin, A. Ayral, The dual effect of Mg on the long-term alteration rate of AVM nuclear waste glasses, Journal of Nuclear Materials, 427 (2012) 297-310.

[43] E. Curti, J.L. Crovisier, G. Morvan, A.M. Karpoff, Long-term corrosion of two nuclear waste reference glasses (MW and SON68): A kinetic and mineral alteration study, Applied Geochemistry, 21 (2006) 1152-1168.

[44] H. Aréna, N. Godon, D. Rébiscoul, R. Podor, E. Garcès, M. Cabie, J.P. Mestre, Impact of Zn, Mg, Ni and Co elements on glass alteration: Additive effects, Journal of Nuclear Materials, 470 (2016) 55-67.

[45] Y. Marcus, Thermodynamics of solvation of ions. Part 5.—Gibbs free energy of hydration at 298.15 K, Journal of the Chemical Society, Faraday Transactions, 87 (1991) 2995-2999.

[46] A. Perez, D. Daval, M. Fournier, M. Vital, J.-M. Delaye, S. Gin, Comparing the reactivity of glasses with their crystalline equivalents: The case study of plagioclase feldspar, Geochimica et Cosmochimica Acta, 254 (2019) 122-141.

[47] C.L. Corkhill, A.J. Fisher, D.M. Strachan, R.J. Hand, N.C. Hyatt, Corrigendum to “The dissolution rates of simulated UK Magnox – ThORP blend nuclear waste glass as a function of pH, temperature and waste loading” [Miner. Mag. 79, (2015) 1529–1542], Mineralogical Magazine, 82 (2018) 939-942.

[48] S.A. Walling, M.N. Kauffmann, L.J. Gardner, D.J. Bailey, M.C. Stennett, C.L. Corkhill, N.C. Hyatt, Characterisation and disposability assessment of multi-waste stream in-container vitrified products for higher activity radioactive waste, Journal of Hazardous Materials, (2020) 123764.

[49] D.M. Strachan, W.W. Schulz, Characterisation of pollucite as a material for the long term storage of Cesium-137 (ARH-SA-294), in, Atlantic Richfield Hanford Company, Richland, Washingtn, 1977.

[50] H.L. Finston, M.T. Kinsley, The radiochemistry of cesium, in, Brookhaven National Laboratory, New York, USA, 1961.

[51] Y. Yokomori, K. Asazuki, N. Kamiya, Y. Yano, K. Akamatsu, T. Toda, A. Aruga, Y. Kaneo, S. Matsuoka, K. Nishi, S. Matsumoto, Final storage of radioactive cesium by pollucite hydrothermal synthesis, Scientific Reports, 4 (2014) 4195.

[52] E.R. Vance, B.E. Scheetz, M.W. Barnes, B.J. Bodnar, Studies of pollucite, in: MRS Proceedings, 1981.

[53] K. Yanagisawa, M. Nishioka, N. Yamasaki, Immobilization of cesium into pollucite structure by hydrothermal hot-pressing, Journal of Nuclear Science and Technology, 24 (1987) 51-60.

[54] S. Komarneni, R. Roy, Hydrothermal reaction and dissolution studies of $CsAlSi_5O_{12}$ in water and brines, Journal of the American Ceramic Society, 66 (1983) 471-474.

603 [55] R. Harjula, E. Tusa, R. Koivula, Performance of zeolite, silicotitanate, CsTreat® and SrTreat® ion
604 exchange materials in Fukushima clean up, in: WM2017 Conference, Phoeniz, AZ, 2017, pp. 17114.

605 [56] N.C. Hyatt, C.L. Corkhill, M.C. Stennett, R.J. Hand, L.J. Gardner, C.L. Thorpe, The HADES facility for high
606 activity decommissioning engineering & science: Part of the UK national nuclear user facility, IOP
607 Conference Proceedings: Materials Science and Engineering, 818 (2020) 012022.

608